Earth Sciences
2018; 7(5): 216-226
http://www.sciencepublishinggroup.com/j/earth
doi: 10.11648/j.earth.20180705.13
ISSN: 2328-5974 (Print); ISSN: 2328-5982 (Online)

Coupled Flow Simulation and Geomechanical Modeling on CO_2 Storage in a Saline Aquifer

Lu Ji

Sinopec Star Petroleum Corporation Limited, Beijing, China

Email address:
lj_uk17@hotmail.com

To cite this article:
Lu Ji. Coupled Flow Simulation and Geomechanical Modeling on CO2 Storage in a Saline Aquifer. *Earth Sciences*. Vol. 7, No. 5, 2018, pp. 216-226. doi: 10.11648/j.earth.20180705.13

Received: July 23, 2018; **Accepted**: September 3, 2018; **Published**: September 28, 2018

Abstract: As an option to mitigate the increasing level of greenhouse gas emission, a number of Carbon Capture and Storage (CCS) testing and pilot projects have been brought up all over the world. In general, there are three types of CO_2 storage formations, such as deep saline aquifers, depleted oil and gas reservoirs, and un-mineable coal seams. This study is focused on the deep saline aquifer which has the largest potential for CO_2 storage. There are a lot of uncertainties associated with this type of storage, such as storage capacity, geomechanical properties, and sealing behaviour of the caprock. Pressure (and temperature) changes during CO_2 injection and storage can have significant impact on the stress and strain field and may cause relevant geomechanical problems. This paper shows a case study of a synthetic saline aquifer storage site, where a 15-year injection at a rate of 15 MT/year was simulated. Sealing performance and leakage risk were evaluated. A number of sensitivity studies were conducted to analyse the impacts of different rock properties on CO_2 leakage potentials. Coupled flow simulation and geomechanical modeling was performed to monitor stress-strain evolutions and to predict failure potentials in response to pressure changes during CO_2 injection and storage. The findings show that CO_2 leakage is most sensitive to caprock permeability. Other factors such as reservoir properties, boundary conditions, and perforation intervals also have certain degree of influence on the leakage. During the 15-year injection, there is no significant risk of potential failure; however, this may happen in local area due to formation heterogeneity.

Keywords: CO_2 Storage, Flow Simulation, Geomechanical Modeling, Saline Aquifer

1. Introduction

With increasing global concerns about the greenhouse effects on climate change, CCS has become a hot research topic as being one of the potential atmosphere mitigation options. CCS is the abbreviation for carbon dioxide capture and storage, and covers a series of procedures from the separation, compression and transportation of CO_2 from industrial and energy-related sources, to the injection and long-term storage in the subsurface [1-3].

Geomechanics plays a vital role on the whole workflow of CO_2 storage [4-6]. Pressure (and temperature) changes during CO_2 injection and storage can have significant impact on the stress and strain field. Figure 1 demonstrates different geomechanical issues that may happen during CO_2 injection and storage [4].

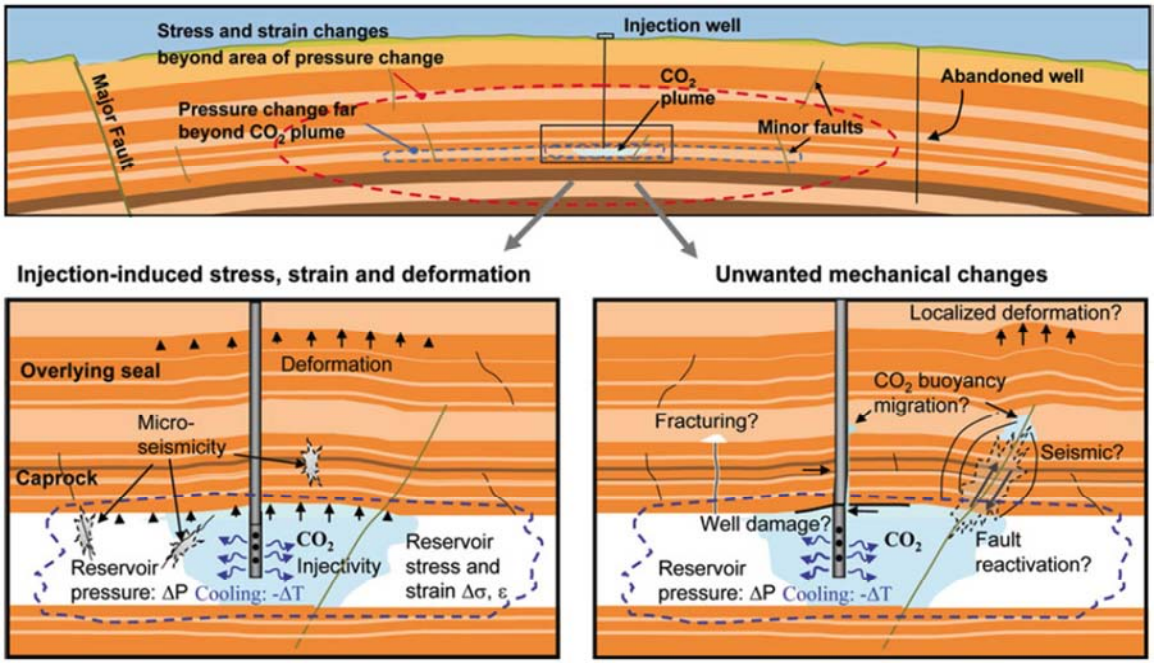

Figure 1. *Geomechanical issues related to CCS [4].*

Near injection area, upward ground deformation in the overburden, micro-seismicity inside and outside of injection formation, fracture and fault re-activation, well damage and other unforeseen damages may happen in response to the pressure and temperature changes. Stress-strain changes can be transmitted into a far extent of area and alter the stress state over there. Minor faults and fractures may be initiated. These harmful geomechanical events in turn will influence the storage efficiency and security. Sometimes the magnitude may be large enough to cause public concerns, and finally fail the entire project [4, 5, 6].

To prevent and predict these unwanted geomechanic issues, a good risk assessment should be done before the initiation of the injection. Moreover, a proper designed monitoring system should be deployed over the entire period of storage. Lessons which have been learned from previous and current existing projects, such as the In Salah project, should be well involved into the design of future projects [5, 7, 8].

In this study, failure criteria and coupled flow and geomechanical simulation will be discussed in the light of giving predictions on potential failure events.

2. Data Summary

2.1. Introduction to the Area of Study

The base model for this study was constructed based on a hypothetic onshore site in Lincolnshire (England). It has relatively horizontal beds dipping (1^o-2^o) eastwards to the offshore. Sub-vertical faults are seen in the central part, with fault throws range from 10 to 50 meters [9]. Formations of caprock, reservoir and basal rock are Sherwood Sandstone Group (SSG), Mercia Mudstone Group (MMG), and Roxby Mudstone Formation (RMF) respectively [9].

2.2. Simulation Model Overview

The geological model was provided by British Geology Survey as part of the CO_2 Aquifer Storage Site Evaluation and Monitoring project (CASSEM). The geological model was constructed based on seismic and well log interpretations [9]. The base model occupies an area of 52m x 52m approximately, including the caprock, aquifer and basal rock formations (Figure 2). Vertically, this model has an average thickness of 600m, extending from 250m to 1665m.

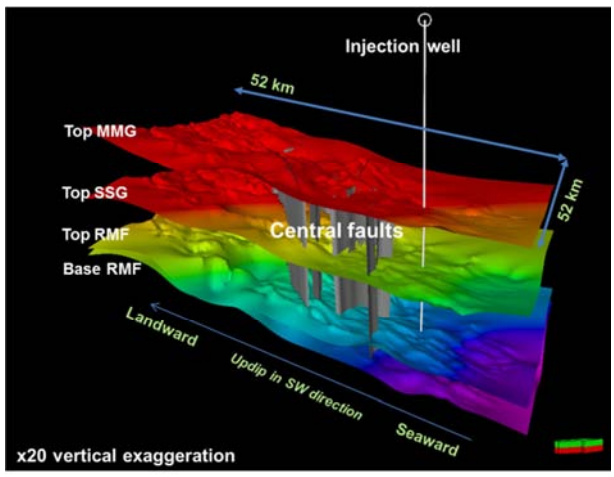

Figure 2. *The geological model of the Lincolnshire injection site.*

Rock properties and fluid properties came from borehole and core measurements. Data from published papers were also included for the information of relative permeability and capillary pressure.

Table 1 displays the main properties in the base model. The total grid cell number is 96480, with 96x67x15 in the I-

J-K directions respectively. Horizontal cell size is 450m by 450m. The top three layers act as the cap rock – MMG. Aquifer formation starts from layer four and extends until layer fourteen. Finally, the bottom layer represents the basal rock – RMF. Petrophysical properties were populated by Sequential Gaussian Simulation (SGS) method [10]. The injection and storage of CO2 was simulated in Eclipse300 based on the CO2STORE Module [11].

Table 1. *LINCS model parameters.*

Model area (km x km)		52 x 52
Model thickness (m)		600
Cell size in horizontal (m)		450
Range of cell size in vertical (m)		0.03-200
	Cap rock	0.1
Porosity (fraction)	Aquifer rock	0.21
	Basal rock	0.03
	Cap rock	0.005
Kh (mD)	Aquifer rock	500
	Basal rock	0.005
Kv/Kh		0.1
NTG		0.9

Capillary pressure was calculated through the Brookes-Corey equation for the reservoir formation [11], and then scaled for the non-reservoir formations using Leverett's scaling rule [12]. During the base case flow simulation, supercritical CO_2 was injected into the saline aquifer from a single well at a rate of 15 MT/year for 15 years. At the end of the injection, this well was shut in and an afterwards CO_2 storage was simulated for 7000 years to monitoring the CO_2 migration, pressure distribution and stress-strain changes.

3. Methods & Workflow

Table 2. *Simulation cases in sensitivity study.*

No.	Case parameters
0	Base model
1	Non-reservoir permeability (*100)
2	Non-reservoir permeability (/100)
3	Reservoir permeability (*10)
4	Reservoir permeability (/10)
5	Non-reservoir porosity (*5)
6	Non-reservoir porosity (/5)
7	Reservoir porosity (*1.2)
8	Reservoir porosity (/2)
9	Closed boundary
10	Perforation at bottom
11	Wells (1MT/year)

Injected CO_2 typically exists in three different phases: free flowing mobile phase, residually trapped immobile phase, and dissolved aqueous phase [13]. This study focuses on the potential CO_2 leakage from saline aquifer formations to the immediate caprock in all three phases. Two types of leakage mechanisms have been considered: first one is the leakage through natural pore throats; second one is the leakage through re-activate fractures and faults.

3.1. CO_2 Leakage Through Intact Caprock

In this study, the term 'CO_2 leakage through intact caprock' refers to all the forms of CO_2 found in caprock during injection and storage. Immobile CO_2 can be found trapped in caprock by capillary pressure. Mobile CO_2 can be found in the pore throats of caprock when it overcomes the capillary pressure. Dissolved CO_2 can also exist in caprock due to solubility. Darcy's law is usually applied in the analysis of fluid flow in porous media. According to its equation, permeability, pressure gradient, and fluid viscosity are three main influencing factors. Capillary pressure is linked with porosity and permeability according to Leverett's scaling rule [12]. So it was varied by a certain factor at the same time when porosity and permeability were changed.

The provided simulation model was used as base case; a number of sensitivity tests based on it were performed to check the impact from different model parameters as listed in Table 2. Here, we assumed the porosity and permeability of caprock and reservoir rock to be independent properties, so the change of one property didn't change the magnitude in another one. The upper and lower bound of the main rock properties were decided from a combination of published literatures in this area. Possible formation fracturing was also taken care of by setting a maximum injection pressure. Base case assumed an open aquifer condition by including numerical aquifers in the boundary. In sensitivity Case 9, closed boundary condition was investigated. Each well is located about 1km apart from its neighbour with the base case well at the centre. Gravity effect and the buoyancy of CO_2 plum was tested where the perforation interval was set at the bottom of aquifer rather that the entire aquifer interval in the base case. In terms of injection rate, base case assumed a rate of 15 MT per year from just one well; however, this number is not realistic for a CCS project. It was suggested to use 1MT per well per year instead, thus 15 wells at this injection rate were replaced in Case11.

More detailed sensitivity simulations have been done by [14]. They ranked parameters according to its effect on the so-called leakage ratio which was defined by the following equation:

$$\text{Leakage ratio} = 10^{(29.7193 - 17.3611*\text{lt} + 2.8106*\text{lk} - 28.9476*\text{p} - 0.8516*\text{lkr})} \quad (1)$$

Their results suggest that caprock thickness and permeability have the first order influence, and the rest of parameters have the second and third order of influences on leakage ratio.

3.2. CO_2 Leakage Through Deformed Caprock and Reservoir

The key parameters in a geomechanical study include pore

pressure, elastic properties, rock strength and principle stresses. Information of principle stresses such as orientation and relations can be obtained from the in situ or global tectonic stress field. Most of the elastic properties and rock strength data could be derived from laboratory tests. The elastic moduli from laboratory test usually refer to static moduli, and they are input for geomechanical model. It should be distinguished from the dynamic moduli which are calculated from the elastic wave properties (e.g. velocity and density). They could differ a lot especially for the weak rock [15]. The relation between the two has not been well defined so far. In this study, a combination of static and dynamic moduli was used, and this could introduce uncertainty to our modeling results.

3.2.1. Tensile Failure

Tensile failure could happen when the maximum injection pressure reached the fracture pressure. This usually tends to happen near well location. Empirical relations have been developed for the calculation of fracture pressure, such as the Hubbert and Willis equation [16], Matthew and Kelley Correlation, Pennebaker Correlation, Eaton's Correlation, and Christman Correlation [17]. Eaton's equation was used in this study for fracture pressure calculation:

$$P_{frac} = P_p + \frac{\nu}{1-\nu}(S_V - P_p) \quad (2)$$

Where Pp is the pore pressure, S_V is the vertical overburden stress, and ν is the Poisson's ratio. Assume a normal vertical stress gradient 1psi/ft in the overburden, S_V can be calculated for each depth.

3.2.2. Shear Failure

Mohr-Coulomb criterion was used for predicting shear failure in this study by assuming the faults to be cohesionless. The frictional limit can be defined by the Jaeger and Cook Equation for strike-slip faulting [18]:

$$\frac{\sigma_1'}{\sigma_3'} = \frac{S_H - P_p}{S_h - P_p} \leq \left[(\mu^2+1)^{1/2} + \mu\right]^2 \quad (3)$$

Where σ_1' is the maximum effective stress, σ_3' is the minimum effective stress, S_H is the maximum horizontal pressure, S_h is the minimum horizontal pressure, and μ is the coefficient of friction. The range of μ is between 0.6 and 1 according to the Byerlee's law. In this way, the critical ratio of the maximum and minimum effective stress can be calculated.

3.3. Project Workflow

Figure 3 is a summary of the project workflow.

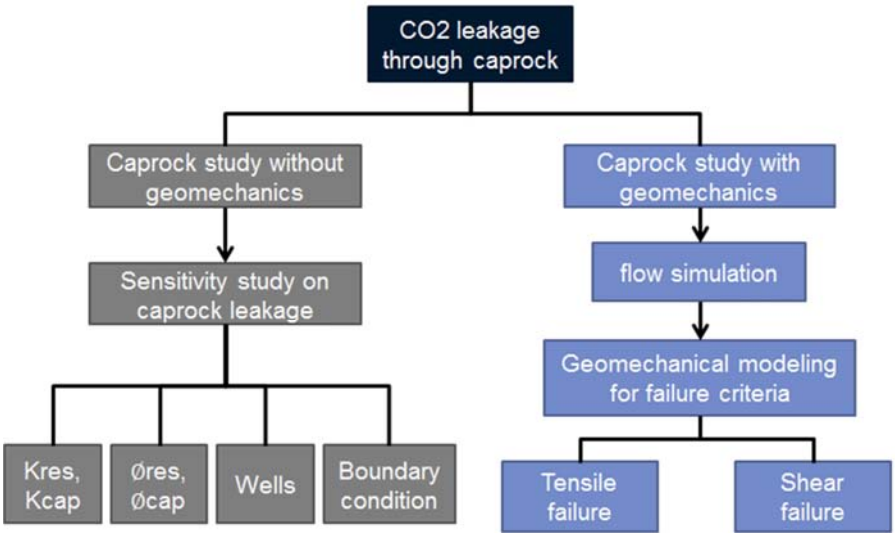

Figure 3. *Project workflow.*

4. Dynamic Simulation and Results Interpretation

4.1. Sensitivity Study of CO_2 Leakage into Intact Caprock

As described in section 3.1, all the simulation cases were run by ECLIPSE 300. Figure 4 illustrate the proportion of CO_2 in mobile, immobile, and dissolved phases respectively at the end of 15-year injection. The most significant difference is observed in Case 11. More CO_2 was dissolved into water because of an increased number of injectors. This in turn increased the contact between CO_2 and saline aquifer. There was more trapped CO_2 in this case as well due to the lower injection rate; thus pressure build-up around the well was not big enough to push CO_2 moving forward freely.

Figure 5 shows the proportions of different phase of CO_2 at the end of 7000-year storage. There was very little CO_2 remaining in mobile phase, only about 2%. The rest of CO_2 remained trapped (68%-78%) or dissolved (20%-32%). The only exception is in Case 3, where the dissolved phase is dominant with a proportion of 66%. This is because CO_2 plume travelled longer distance in the high perm aquifer formation.

Until now we have looked at average behaviours in the

whole model, next we will discover the impact on caprock sealing performance. Total amount of CO_2 within caprock including mobile, immobile, and dissolved CO_2 was normalised against the base case result, and was plotted using logarithmic scale. Figure 6 summarizes the total amount of CO_2 in three phases within caprock both at the end of injection and at the end of simulation, and all the results were normalised against the base case. This gives a clearer view of the impact from each parameter. The model parameters can be ranked from the most influenced to the least influences factor as: non-reservoir permeability, reservoir permeability, porosity, boundary effects, and injection rate.

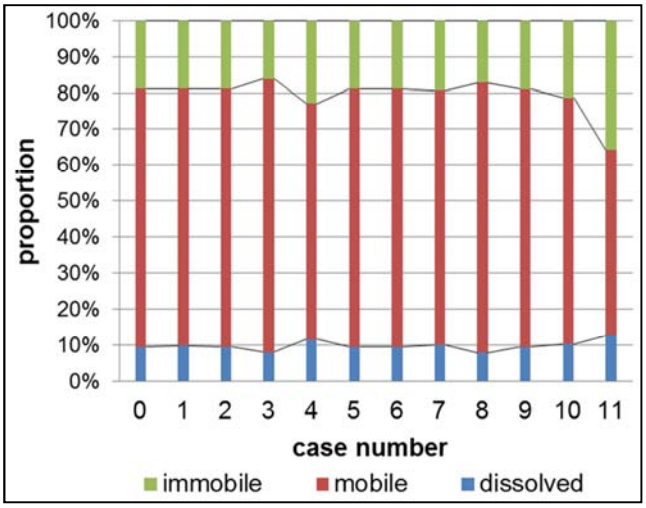

Figure 4. *Proportion of CO_2 in three phases at the end of injection (the 15th year).*

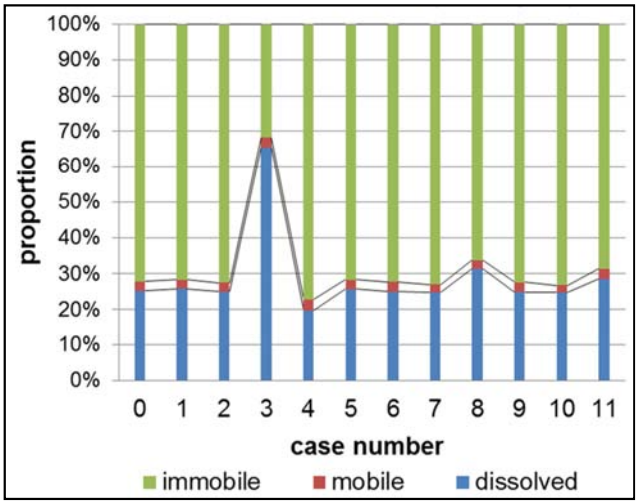

Figure 5. *CO_2 distributions at the end of simulation (the 7015th year).*

The total molar amount of dissolved CO_2 in the basal rock was plotted in Figure 7. Significant amount of CO_2 was dissolved in the underburden in Case 4 and 9. The decrease of reservoir permeability held back the buoyancy of CO_2, pressure build-up near well and at bottom due to gravity and more CO_2 dissolved in saline aquifer. The increase of basal rock permeability also decreased its capillary entry pressure. Figure 8 shows the huge pressure build-up at bottom of reservoir and this acted as a force to push CO_2 into underburden and finally dissolved into water phase.

4.2. Coupled Geomechanical Modeling in Petrel 2013

The simulation results (pressure changes) of Case 11 were used in the following coupled geomechanical modeling.

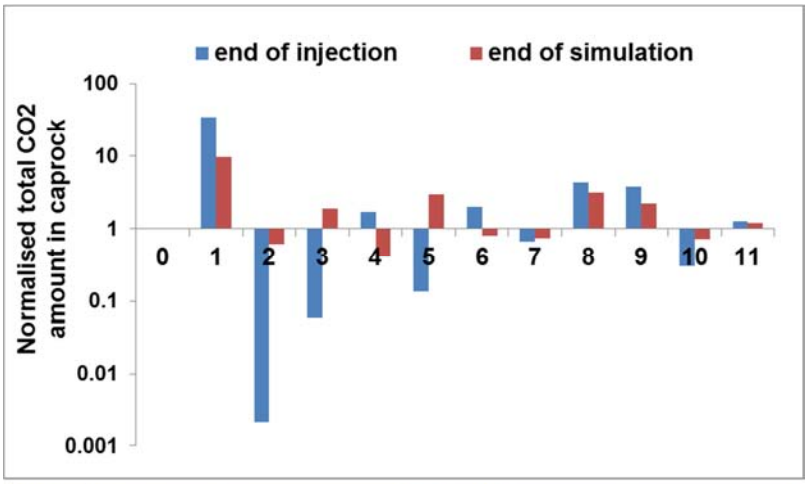

NO.	Case parameters	NO.	Case parameters
0	Base model	6	Non-reservoir porosity (/5)
1	Non-reservoir permeability (*100)	7	Reservoir porosity (*1.2)
2	Non-reservoir permeability (/100)	8	Reservoir porosity (/2)
3	Reservoir permeability (*10)	9	Closed boundary
4	Reservoir permeability (/10)	10	Perforation at bottom
5	Non-reservoir porosity (*5)	11	15 Wells (1MT/year)

Figure 6. *Normalised total amount of CO_2 within caprock.*

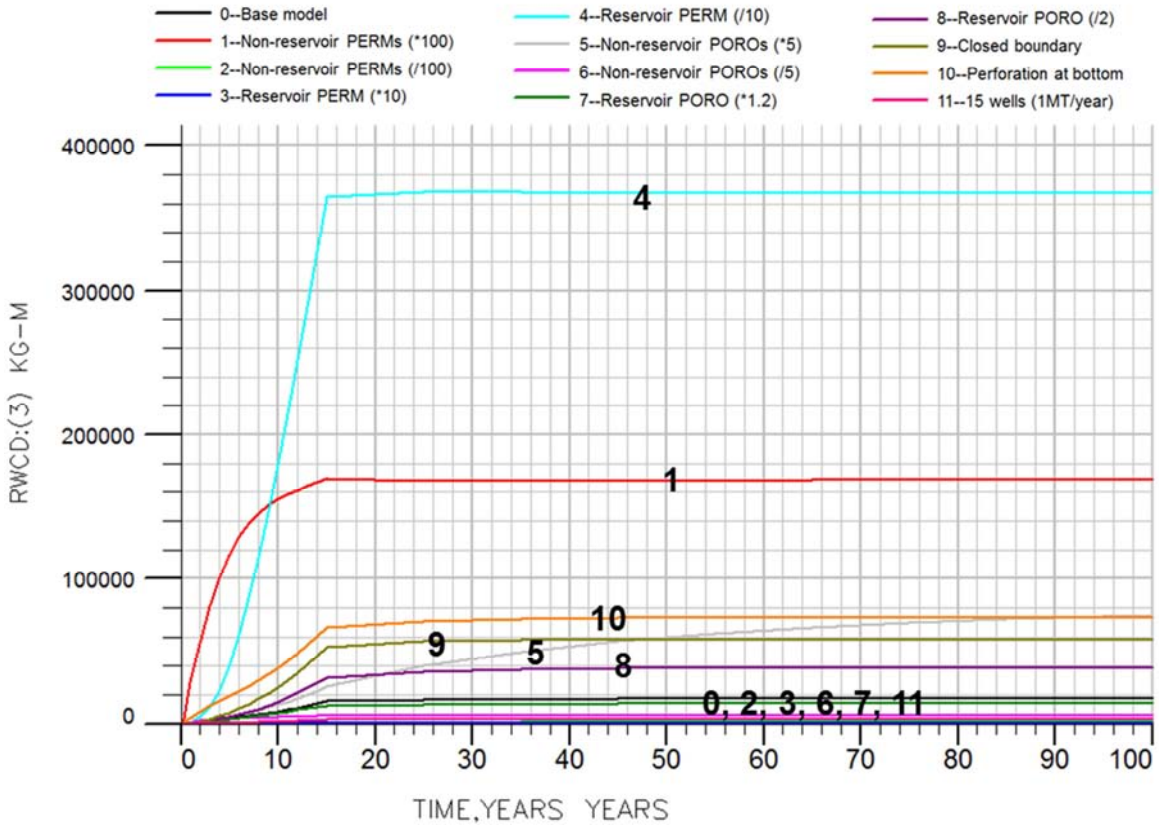

Figure 7. *Dissolved CO_2 within the basal rock region.*

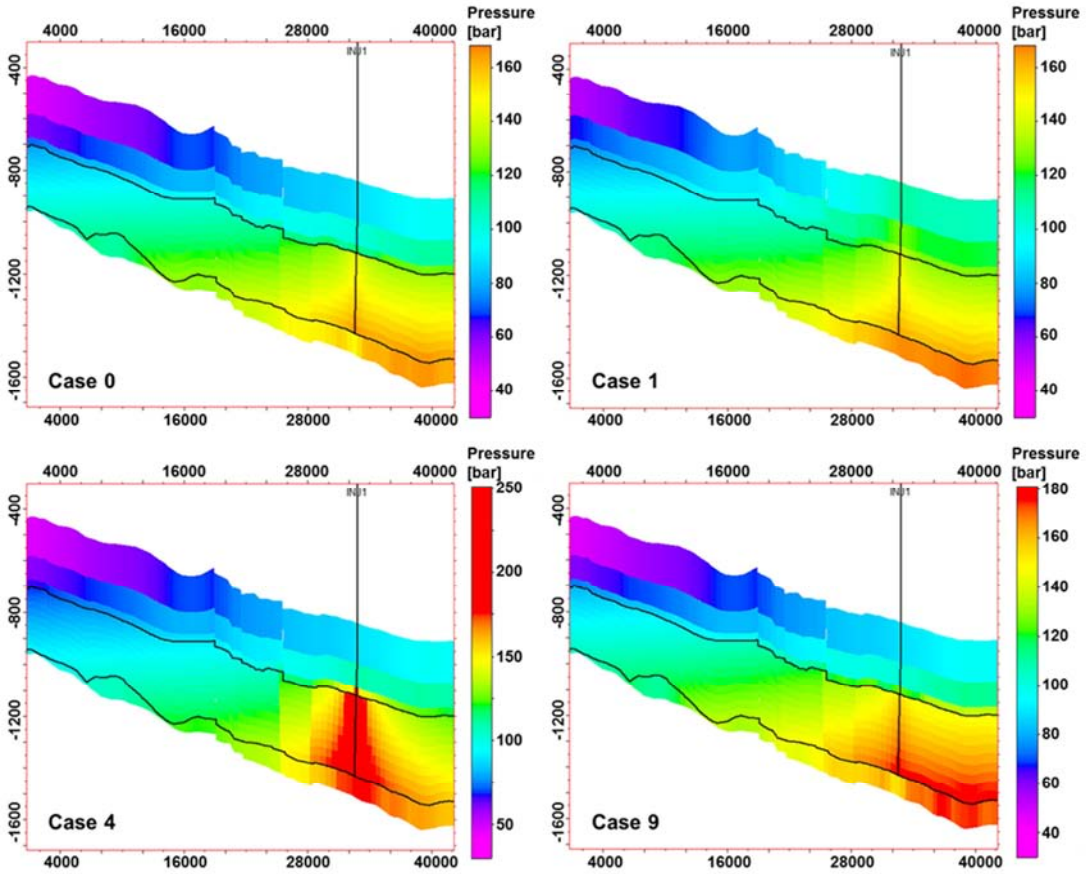

Figure 8. *A cross-section view of pressure distribution at the end of 10-year injection for Case 0, 1, 4, and 9.*

4.2.1. Make Geomechanical Grid

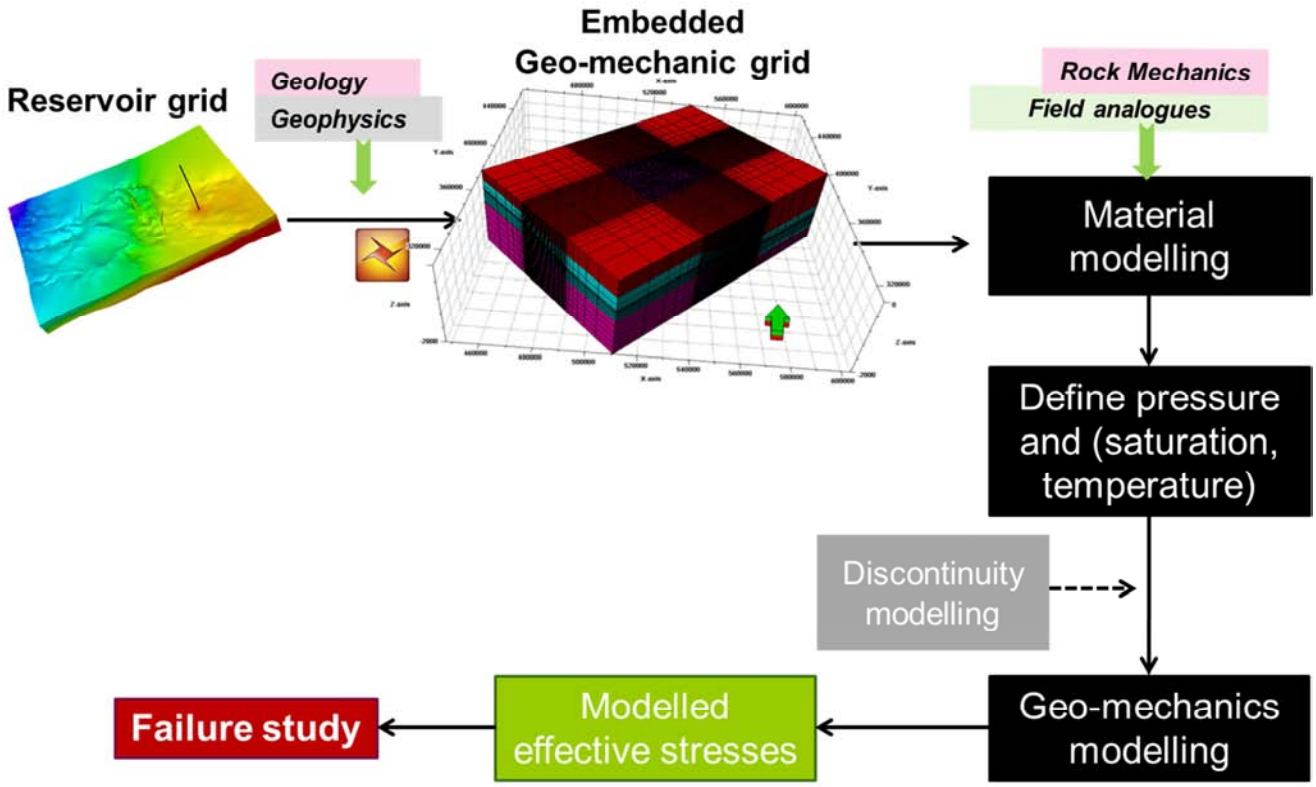

Figure 9. *Geomechanical modeling workflow.*

Figure 9 displays each step inside geomechanical modeling through the Reservoir Geomechanics Module in Petrel 2013. Model grid and simulation results (e.g. pressure) from Eclipse 300 simulator were imported into Petrel 2013. Next, the model grid was embedded in all directions. Seven layers of equal thickness were added above the model to extend the overburden to surface at 0m. Six layers of equal thickness were added underlying to extend the underburden to the depth of 2000m. Laterally, seven cells with increasing size by a factor of 1.5 were added in each direction to serve as sideburdens and this will reduce the boundary effects during simulation. The final geomechanical grid has an angle against the global axes due to the nature of simulation grid. Grid rotation was tried to make it in accordance with global axes, however, this made a great impact on the distributions of properties. The reason is because properties are assigned to each cell; rotation of the grid will relocate cells and eventually change the property distributions. So it is essential to keep the grid orientation the same as simulation model. After embedding, the total number of grid cell reaches 249480 (110*81*28). It is suggested to reduce the cell number through simulation model upscaling; however, this means a start over from the beginning. For the concerns of short period of time, upscaling was not performed, and geomechanical modeling was carried on with the original grid.

4.2.2. Material Modeling

Next step is material modeling; different mechanical properties as described in section 3.2 were assigned with a proper value to each lithology. Usually, laboratory rock mechanic tests are designed to estimate the magnitude of these parameters or give correlations with other parameters (e.g. velocity, porosity, and density). In the case of no lab tests, published values could also be used as an analogue and tuned by calibration with stress and strain observations which will be talked about in the following uncertainty section. As described in [19], published correlations with porosity for both shale and sandstone were applied, and then the derived values were shifted according to the data from mechanical tests. In this study, mechanical properties were calculated in the same way. The only difference is an average value was used for each lithology rather than a distribution. It is because the porosity was populated through SGS, the distribution could be different from the real case. By using average value, uncertainty could be reduced to some degree. Mechanical properties in this model are listed in Table 3.

Table 3. *Mechanical properties used in this study.*

Layer No.	Forma tion	Young's Modulus(GPa)	Poisson's Ratio	Biot's constant	Bulk Density	Porosity	Angle of friction
1 to 7	Over-burden shale	3	0.3	1	1.9	0.3	55
8 to 10	MMG	4.21	0.12	1	2	0.1	26
11 to 21	SSG	15.5	0.25	1	2.6	0.21	35
22	RMF	1.33	0.12	1	2.2	0.03	15
23 to 28	Under-burden shale	22	0.25	1	2.4	0.01	11

Porosity and density for the overburden above Mercia mudstone and the underburden below Roxby mudstone were taken from general values for shallow and deep shales. Porosity for MMG, SSG, and RMF were taken from model properties. Density for the three formations was taken from published papers for each formation [20]. Biot's constant was assumed to be 1 for all the cases.

4.2.3. Initial In-situ Stress and Boundary Condition

Stress initialization method was used for the model boundary condition. The information for in-situ maximum horizontal stress was taken from the World Stress Map database.

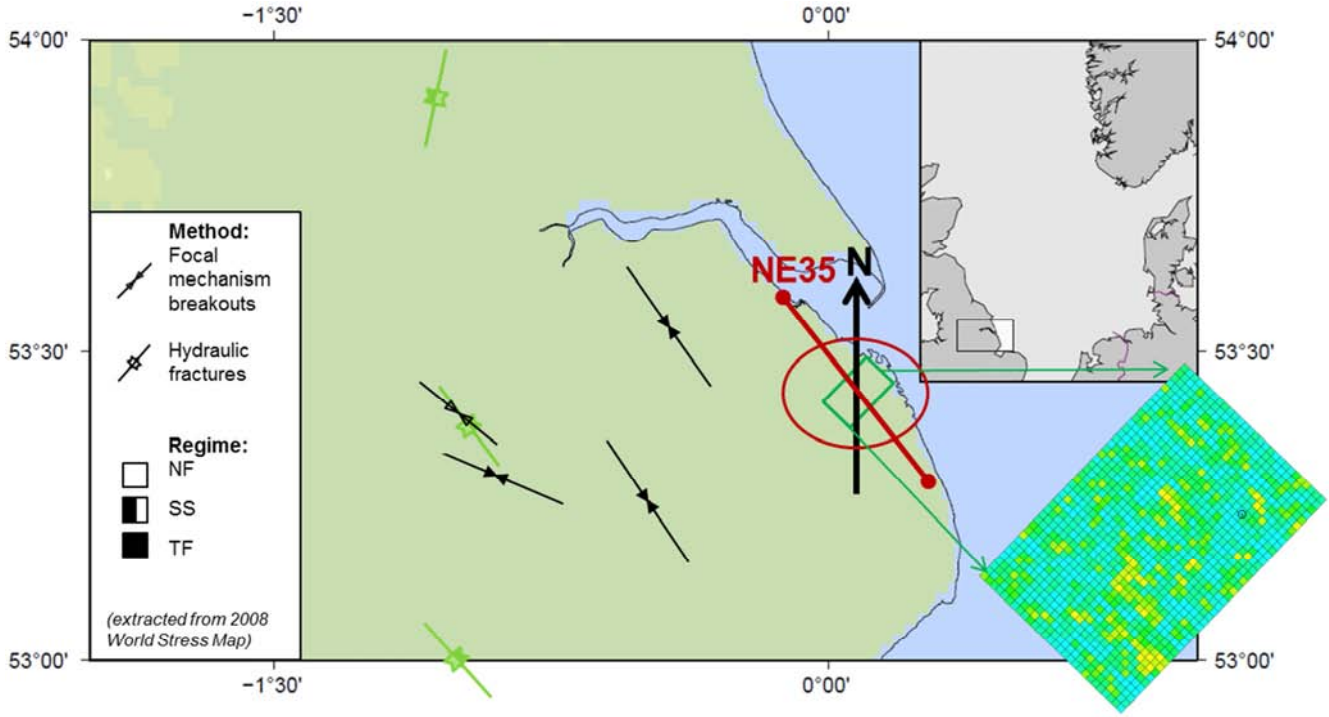

Figure 10. *In situ maximum horizontal stress direction and stress regime (generated from world-stress-map website).*

Figure 10 displays the maximum horizontal stress measured from various methods as describe in Zoback's book [21]. The injection site is pointed out by green box. There is no data around its location, so the nearest one which has an orientation of NE35° was assumed to be the applicable for this site. The stress regime for this model was following strike-slip similar as the ones to the west of this site. The strike-slip regime represents a stress state where the maximum principle stress (S_1) is the maximum horizontal stress (S_H), and the minimum principle stress (S_3) is the minimum horizontal stress (S_h) according to Anderson's classification. Fault will initiate when the then difference between the maximum and minimum principle stress become very large. The relationship among the three principle stresses was assumed as following [22]:

$$S_H = 1.5S_V = 1.5S_h \quad (4)$$

4.2.4. Geomechanical Modeling and Failure Prediction

The time-step in geomechanical modeling was scheduled to be every 5 years in the injection period and every 1000years in the storage period. As described in section 3.2.3, the Mohr-Coulomb criterion was used here to analyse shear failure. Taking the lower bound of friction coefficient of 0.6 from Byerlee's Law [21], the ratio of the maximum and minimum effective stress (σ_1' and σ_3') should be less than 3 to prevent shear slip.

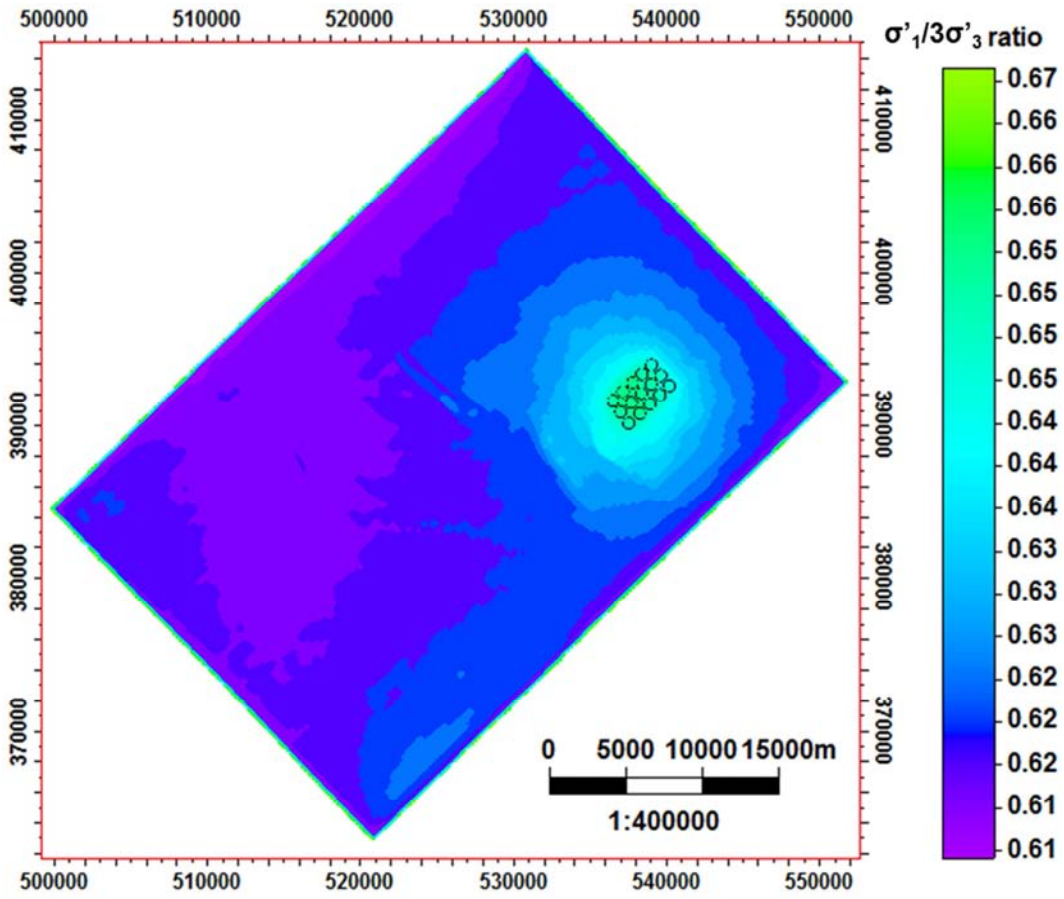

Figure 11. *Shear failure potential map of top aquifer layer at the end of injection.*

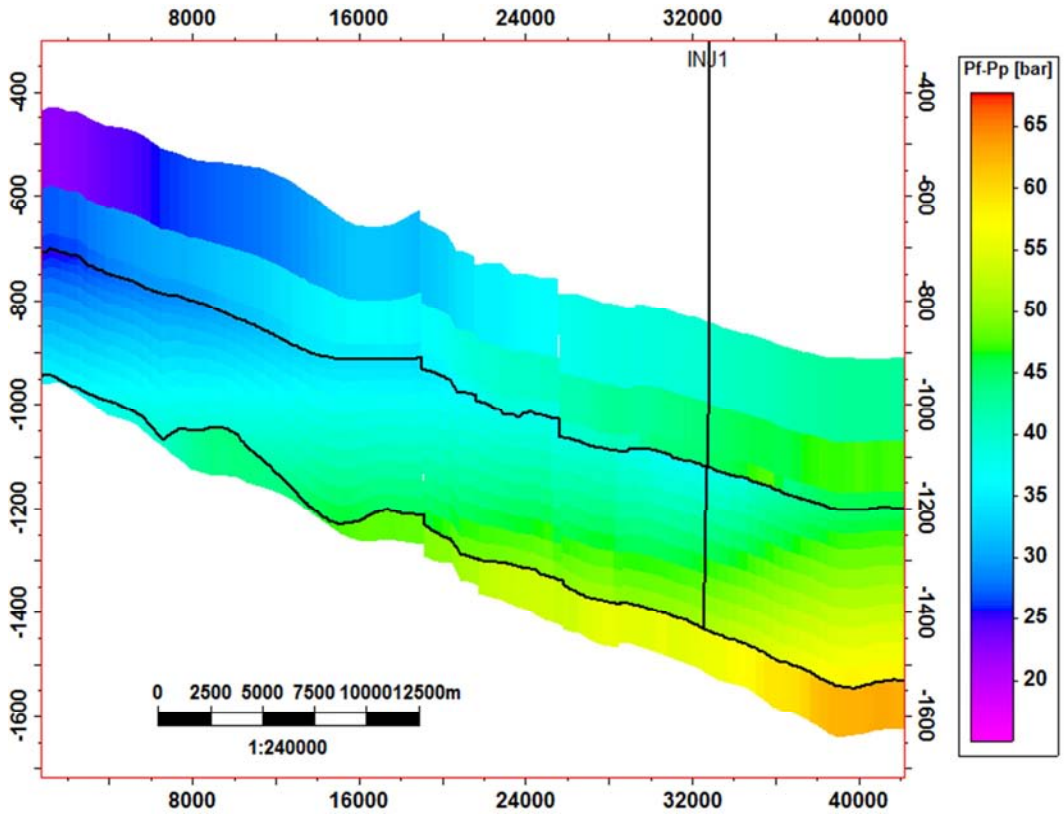

Figure 12. *Cross-section view of tensile failure potential at the end of injection.*

Figure 11 shows the shear failure potential in the top layer of aquifer at the end of 15-year injection. This value was also checked in the caprock, basal rock and other intervals inside aquifer. It is found that all of these intervals have a shear failure potential less than 1, which is indicating that no shear failure happened by that time. After injection stopped, the high pressure around the injection area will equilibrium in the whole field and no fault re-activation will likely to happen during this period.

Tensile failure is very unlikely to happen as the maximum injection pressure was set to be lower than the fracture pressure. However, it will be better to double check on the pressure distribution against the calculated fracture pressure. Fracture pressure for each depth was calculated using the Eton's equation.

Figure 12 is a cross-section view of the difference between fracture pressure and pore pressure at the end of 15-year injection, negative values indicate tensile failure, and positive values indicate no tensile failure. It can be concluded that no tensile failure during the injection period.

5. Conclusions and Suggestions for Future Work

In this study, the principles of CO_2 leakage have been discussed in two directions. The effect on intact caprock leakage was looked at by conducting a series of sensitivity simulations. For this specific site, it is found that caprock permeability plays the most important role in CO_2 leakage; reservoir properties, boundary conditions and well parameters have limited but non-negligible effects on this. In general, leakage through intact caprock is very little compared to the amount of injection. Escaped CO_2 in the caprock tends to be dissolved into formation water and trapped by capillary pressure. Only in the condition of very permeable caprock, mobile CO_2 was seen in the lower interval of caprock.

Coupled flow simulation and geomechanical modeling was performed to monitor potential failures in response to pressure changes during CO_2 injection and storage. During 15 years injection, there was no risk of potential geomechanical failure when average mechanical properties were used; however it may happen in local area due to formation heterogeneity.

The biggest uncertain related with this study is from the lack of field data. Most of the petrophysical and mechanical properties were taken from analogue data or empirical correlations. The properties of caprock should be taken great care of since it has big influence of storage efficiency. Petrophysical properties of shales determined from correlations may be error-prone because the mineral contents vary a lot for different type of shales. Correlations derived from mechanical tests for caprock are weak as there's no sufficient core plugs provided. The result could bias if the formation tend to be heterogeneous.

The geomechanical model should be calibrated in future when more field data will be available. These data could come from compaction logs obtained at well location, ground deformations from satellite imaging, observed failure events, 4D seismic, etc. The calibrated geomechanical model can be more applicable for future predictions on storage behaviour.

Temperature may also be coupled into geomechanical analysis to study the cooling effects on the rock deformations.

Acknowledgements

Many thanks to Gillian Pickup and Peter Olden for their technical support and advices regarding to this project. Special thanks to Edinburgh Time-Lapse Project research team for their support in finishing this study.

References

[1] Eccles J.K., and R.S. Middleton, 2018, Large-Scale Energy Infrastructure Optimization: Breakthroughs and Challenges of CO2 Capture and Storage (CCS) Modeling. In: Thill JC. (eds) Spatial Analysis and Location Modeling in Urban and Regional Systems. Advances in Geographic Information Science. Springer, Berlin, Heidelberg, doi: 10.1007/978-3-642-37896-6_14.

[2] Underschultz, J., D. Kevin, M. Karsten, S. Sandeep, W. Terry, and W. Steve, 2017, Carbon capture and storage, Sustainability in the mineral and energy sectors, United States: Taylor & Francis Group, p. 437-452, doi: 10.1201/9781315369853-24.

[3] Metz, B., O. Davidson, H. De Coninck, M. Loos, and L. Meyer, 2005, IPCC Special Report on Carbon Dioxide Capture and Storage: Cambridge University Press, doi:10.1021/es200619j.

[4] Rutqvist, J., 2012, The Geomechanics of CO2 Storage in Deep Sedimentary Formations: Geotechnical and Geological Engineering, v. 30, no. 3, p. 525–551, doi: 10.1007/s10706-011-9491-0.

[5] Joshua A., L. Chiaramonte, S. Ezzedine, W. Foxall, Y. Hao, A. Ramirez, and W. McNab, 2014, Geomechanical behavior of the reservoir and caprock system at the In Salah CO2 storage project, PNAS, doi: 10.1073/pnas.1316465111.

[6] Andersen, O.A., H.M. Nilsen, S.E. Gasda, 2017, Vertical Equilibrium Flow Models with Fully Coupled Geomechanics for CO2 Storage Modeling, Using Precomputed Mechanical Response Functions, Energy Procedia, v. 114, p. 3113-3131, doi: 10.1016/j.egypro.2017.03.1440.

[7] Mathieson, A., J. Midgely, I. Wright, N. Saoula, and P. Ringrose, 2011, In Salah CO2 storage JIP: CO2 sequestration monitoring and verification technologies applied at Krechba, Algeria: Energy Procedia, v. 4, p. 3596–3603, doi:10.1016/j.egypro.2011.02.289.

[8] Goodarzi, S., A. Settari, M.D. Zoback, D.W. Keith, 2015, Optimization of a CO2 storage project based on thermal, geomechanical and induced fracturing effects, Journal of Petroleum Science and Engineering, v. 134, p. 49-59, doi: 10.1016/j.petrol.2015.06.004.

[9] Smith, M., D. Campbell, E. Mackay, and D. Polson, 2011, CO2 Aquifer Storage Site Evaluation and Monitoring.

[10] Jin, M., G. Pickup, E. Mackay, A. Todd, A. Monaghan, and M. Naylor, 2010, Static and Dynamic Estimates of CO2 Storage Capacity in Saline Formations, in SPE Europec/EAGE Annual Conference and Exhibition: Society of Exploration Geophysicists, p. SPE131609, doi:10.2118/131609-MS.

[11] Pickup, G. E., M. Jin, P. Olden, E. J. Mackay, and M. Sohrabi, 2011, A Sensitivity Study on CO2 Storage in Saline Aquifers, in SPE EUROPEC/EAGE Annual Conference and Exhibition: Society of Petroleum Engineers, p. SPE143054, doi:10.2118/143054-MS.

[12] Leverett, M. C., 1940, Capillary Behavior in Porous Solids: Spe, v. SPE 941152, p. 152 – 169.

[13] Mathias, S., 2012, ANNEX A2: CO2 Storage Liabilities in the North Sea – An Assessment of Risks and Financial Consequences -- Cap Rock Study.

[14] Hou, Z., M. L. Rockhold, and C. J. Murray, 2012, Evaluating the impact of caprock and reservoir properties on potential risk of CO2 leakage after injection: Environmental Earth Sciences, v. 66, p. 2403–2415, doi:10.1007/s12665-011-1465-2.

[15] Zimmer, M. A., 2003, Seismic velocities in unconsolidated sands: Measurements of pressure, sorting, and compaction effects: Stanford University.

[16] Hubbert, M., and D. Willis, 1972, Mechanics of hydraulic fracturing: Underground Waste Management and Environmental Implications, p. 239–257, doi: 10.1016/S0376-7361(07)53011-6.

[17] Ajienka, J., F. Egbon, and U. Onwuemena, 2009, Deep Offshore Fracture Pressure Prediction in the Niger Delta – A New Approach, in the 33rd Annual SPE International Technical Conference and Exhibition: p. SPE 128339.

[18] Jaeger, J.C., Cook, N.G.W., and R.W. Zimmerman, 1979, Fundamentals of Rock Mechanics: Blackwell publishing.

[19] Olden, P., G. Pickup, M. Jin, E. Mackay, S. Hamilton, J. Somerville, and A. Todd, 2012, Use of rock mechanics laboratory data in geomechanical modelling to increase confidence in CO2 geological storage: International Journal of Greenhouse Gas Control, v. 11, p. 304–315, doi:10.1016/j.ijggc.2012.09.011.

[20] Brook, M., K. Shaw, C. Vincent, and S. Holloway, 2003, GESTCO case study 2a-1: storage potential of the Bunter Sandstone in the UK sector of the Southern North Sea and the adjacent onshore area of eastern England.

[21] Zoback, M. D., 2007, Reservoir Geomechanics: doi:10.11129/detail.9783034615662.38.

[22] Olden, P., J. Min, G. Pickup, E. Mackay, S. Hamilton, J. Somerville, and A. Todd, 2014, Geomechanical modelling of CO2 geological storage with the use of site specific rock mechanics laboratory data: Petroleum Geoscience, v. 20, p. 323–337.